Proc. Natl. Acad. Sci. USA
Vol. 89, pp. 11905–11909, December 1992
Neurobiology

Relationships between orientation-preference pinwheels, cytochrome oxidase blobs, and ocular-dominance columns in primate striate cortex

(cortical modules/vision/topology/optical imaging/intrinsic signals)

EYAL BARTFELD AND AMIRAM GRINVALD

Department of Neurobiology, The Weizmann Institute of Science, Rehovot, 76100, Israel; and Laboratory of Neurobiology, The Rockefeller University, New York, NY 10021

Communicated by Dale Purves, September 3, 1992

ABSTRACT **The relationships between cytochrome oxidase blobs, ocular-dominance columns, and iso-orientation domains, subsystems underlying visual perception, were explored in primary visual cortex of macaque monkey. High-resolution maps of these three subsystems were acquired. Optical imaging based on activity-dependent intrinsic signals revealed that the most prominent organizational feature of orientation preference was a radial arrangement, forming a pinwheel-like structure surrounding a singularity point. More than 80% of these pinwheels were centered along the midline of ocular-dominance columns. The iso-orientation contours of adjacent pinwheels crossed borders of ocular-dominance columns at approximately right angles. Pinwheels with the same or opposite directions of orientation-preference change were smoothly connected with each other. On the average, all orientations were equally represented. In exactly the same cortical area, the cytochrome oxidase blobs, thought to be involved in color processing, were also mapped, using cytochrome oxidase histology. Like the centers of pinwheels, the centers of blobs also lie along the midline of ocular-dominance columns. However, the centers of pinwheels did not coincide with the centers of blobs; these two subsystems are spatially independent. "Hypercolumn" modules, each including two complete pinwheels in two adjacent columns of complementary ocularity, as well as portions of a few blobs, were frequently found but did not seem to be the primary unit of cortical organization. An alternative to hypercolumns is proposed.**

Mountcastle (1) in the cat somatosensory cortex and Hubel and Wiesel (2–4) in the cat and monkey visual cortices have found that cortical cells with similar response properties are frequently clustered together, forming columns (modules) that often traverse the entire cortical depth, from the pia to the white matter. However, the exact organization of different functional modules parallel to the cortical surface still remains an unresolved question for all areas of the mammalian cortex. In macaque monkey primary visual cortex, elaborate synaptic connections endow cortical cells with remarkably selective response properties. Single cells can respond selectively to various types of visual stimuli—e.g., edges or lines of a given orientation, particular colors, specific directions of motion and ocular disparity. Over the last three decades, a functional segregation has been demonstrated for three types of visual-response properties in monkey primary visual cortex. (*i*) The first, and best understood, is the segregation of inputs from the right and the left eye. These segregated inputs form the ocular-dominance columns, which run nearly parallel to one another in slabs that are 400 μm wide (5). (*ii*) A second system of segregated neurons is referred to as the iso-orientation domains (or orientation-preference bands), each domain containing cells that respond best to a given stimulus orientation (6). (*iii*) The third subsystem contains neurons that are thought to be selective for other attributes of the visual stimulus, such as color (7, 8) and spatial frequency (9). These cells are located in the cytochrome oxidase blobs (7–10). Hubel and Wiesel (4) and Livingstone and Hubel (7) have proposed a schematic "ice-cube" model for describing the functional architecture of the repeating "hypercolumns" that contain these three subsystems. However, the exact layout and the relationships between blobs, iso-orientation domains, and ocular-dominance columns have never been determined.

Previous work (1–10) has relied on electrophysiological, anatomical, and histological techniques to reveal the organization of each type of subsystem. Optical imaging (11–14) based on voltage-sensitive dyes (15–20) is a particularly attractive technique for exploring these relations. Blasdel and Salama (21) used voltage-dyes and provided a striking demonstration of the usefulness of optical imaging to study functional architecture in the primate visual cortex. Although they stated that dyes must be used, we have developed an alternative optical-imaging approach (22–24), based on activity-dependent, intrinsic optical changes (23, 25–27), without dyes, to study the functional architecture of visual cortex in anesthetized (24) and awake (28) monkeys. The method has also been used to study the pinwheel-like organization of orientation preference in cat visual cortex (29).

This report establishes the relationships between blobs, pinwheels, and ocular-dominance columns. The architecture reported here, for the upper cortical layers, differs from all other proposed models (4, 7, 21, 30) and sheds light on the issue of hypercolumns in the primary visual cortex (5).

MATERIALS AND METHODS

Animals. Monkeys (*Macaca fascicularis*) were initially anesthetized with ketamine (10 mg/kg, i.m.), followed by sodium pentothal anesthesia (1–3 mg/kg per hr, administered i.v. and supplemented as needed). To monitor the state of the anesthetized monkeys, the electroencephalogram, electrocardiogram, temperature, and expired CO_2 were observed throughout the experiment. To prevent eye movements, the animals were paralyzed with vercuronium bromide (0.2 mg/kg per hr) and artificially respirated.

Imaging Procedure. To minimize pulsation, a sealed, stainless steel chamber was mounted over the exposed cortex. A slow scan charge-coupled device camera (24) was mounted above the optical chamber. The cortical image was projected on this camera using a tandem lens arrangement, which provides high light-collection capability and shallow depth of focus. Thus, by focusing 300 μm below the cortical surface, artifacts from surface blood vessels were largely eliminated

The publication costs of this article were defrayed in part by page charge payment. This article must therefore be hereby marked "*advertisement*" in accordance with 18 U.S.C. §1734 solely to indicate this fact.

(31). The camera provided digitized images of the cortex [eccentricity 6–8°, close to the V1 (area 17)/V2 (area 18) border]. Drifting gratings (6° × 4°) of eight orientations were used (0, 22.5, 45, 67.5, 90, 112.5, 135, and 157.5°). For each 2-sec stimulus, we collected 5–10 frames over a period of 3 sec. The functional maps obtained by optical imaging based on intrinsic signals provide information about the organization of the upper cortical layers with resolution up to 50 μm, down to a depth of ≈600 μm, as discussed elsewhere (20, 23, 24).

Data Analysis. Functional maps can be obtained by comparing the cortical images obtained when the animal views various stimuli. To remove the baseline image and correct for the effects of uneven illumination and other common-mode noise originating from the microvasculature, each of these images is divided by the "blank" image, obtained when the animal viewed a blank screen. The resulting image provides a "single (stimulus) condition" map. To reduce microvascular artifacts even more, in this study, the sum of many images was used instead of the blank. (Images obtained by using many stimulus conditions which activated the cortex uniformly were summed. This sum is referred to as a "cocktail blank.")

"Angle" and "Angle-Magnitude" Maps of Orientation Preference. The detailed organization of orientation preference across the cortical surface can be revealed by analytically comparing several single-condition orientation-preference maps. To calculate the angle maps, showing orientation preference at each pixel in the image, we used vectorial addition (21, 24, 29, 30). Before vectorial addition, single-condition maps of orientation preference were smoothed. In a few experiments, where better maps were generated, smoothing was not done and the results were similar (e.g., ref. 29). Because we used eight stimuli of different orientations, eight such vectors were combined for each pixel, from the responses to the eight stimuli. The resultant vector for each pixel was characterized by its angle and magnitude. These values were used, without smoothing, for displaying the angle and angle–magnitude maps. The latter show the magnitude of the average response, in addition to the angle of orientation preference.

A small magnitude of the resultant vector at a given pixel (21, 24, 30) could arise from three situations: (*i*) the neuronal population monitored by the pixel was poorly activated by all the stimuli, (*ii*) most neurons were activated but, on the average, their responses were not sharply tuned to the stimulus orientations, or (*iii*) an optical artifact, caused by light scattering and out-of-focus blurring, smeared responses from closely spaced locations with different orientation preferences. Inspection of the raw optical data and/or single-unit recordings were used to distinguish between these alternatives.

Orientation Tuning of Neuronal Clusters. To show the orientation tuning of clusters of neurons in a given iso-orientation patch, a histogram was calculated directly from the strength of the individual responses to each of the eight stimulus orientations in each pixel. The histogram was obtained by summing the results for all the pixels in the one-eighth of the imaged cortical area that responded best to a stimulus of a given orientation. This histogram depicts the tuning of a population rather than that of single cells.

Selectivity Index. A selectivity index was calculated in a similar way. (*i*) For each pixel we calculated the orientation-tuning histogram, as before. (*ii*) We calculated the standard polar representation of orientation tuning for each pixel. (*iii*) From this curve we calculated the ratio between long and short axes. A ratio of 1 corresponds to zero orientation selectivity. The full range observed for the tuning strength, monitored by all pixels in the image, was divided into 13 "arbitrary" units. Distribution of selectivity indices seen for the blobs was computed for pixels in all cortical areas covered by blobs. Distribution of the selectivity indices for regions exhibiting preferred responses to an oriented grating (e.g., 90°) was computed from 12.5% of the cortical area, centered around regions that exhibited the strongest responses to this stimulus. Because up to one-fifth of such regions may include blob cells, many of which may not be sharply tuned, this may somewhat degrade the overall orientation tuning of the region.

Reproducibility of Maps. To determine the reproducibility of angle maps, maps obtained from two independent imaging sessions of the same cortical patch were compared. The root-mean-square deviation for the optimal angle detected at each pixel was very small, only 15°. Furthermore, 80% of the singularity points imaged in the two sessions coincided within <30 μm. Small regions of the map that exhibited reduced reproducibility always corresponded to cortical regions with poor selectivity for the set of stimuli used.

Matching Histological Sections with Optical Maps. Proper matching of the post-mortem histological maps with the optical maps obtained *in vivo* is critical in these experiments. To match histological sections with optical maps, we used the locations of lesion sites photographed *in vivo* and markings of three to five injections of 1,1′-dioctadecyl-3,3,3′,3′-tetramethylindocarbocyanine. These techniques facilitated alignment of the sections and correction for tissue shrinkage. We believe that the matching thus obtained was excellent because (*i*) elements of the microvasculature, photographed *in vivo* at high contrast, coincided with venules and arterioles seen in the matched histological section, (*ii*) it is well-known that blobs are centered on ocular-dominance columns, which is what we observed after the matching, and (*iii*) the blobs optically imaged *in vivo*, using a described method (24), coincided with the blobs revealed by the histology.

RESULTS

To optically image iso-orientation domains—i.e., the upper layers of the iso-orientation columns, anesthetized monkeys viewed drifting gratings of various orientations. Using a charge-coupled device camera, optical images of the exposed cortex were taken separately for each stimulus orientation. Fig. 1*A* shows a patch of striate cortex, measuring 1.5 × 1 mm, that was imaged with high resolution, and Fig. 1*B* shows a single-condition iso-orientation map from that region. Eight maps such as that shown in Fig. 1*B* were obtained, one for each of the eight stimulus orientations. These eight maps showed a mosaic-like arrangement for each of the partially overlapping iso-orientation domains. The patchy domains of the various orientation preferences are arranged like flower petals, partially overlapping (data not shown). To provide a detailed picture of the interrelationship among the various iso-orientation domains, we used an analytical procedure (21, 24, 30), that vectorially adds the response strength, for each of the eight stimulus orientations, on a pixel-by-pixel basis. The resultant vector for each pixel is defined by its angle and magnitude, the angle providing the orientation preference at each cortical site. Several types of displays can be used to emphasize various aspects of the architecture of iso-orientation domains; three types will be used here.

The Pinwheel-Like Organization of Orientation Preference. In a "discrete-angle" map (Fig. 1*C*), each color codes for a particular range of orientation preferences. Thus, each color corresponds to an iso-orientation domain represented here with a resolution of 22.5°. The discrete-angle map is useful in showing the direction of iso-orientation contours across the cortical surface. However, it cannot distinguish whether orientation preference changes smoothly or discretely across the cortical surface. These same data, displayed by using a continuous color scale, indicate that orientation preference,

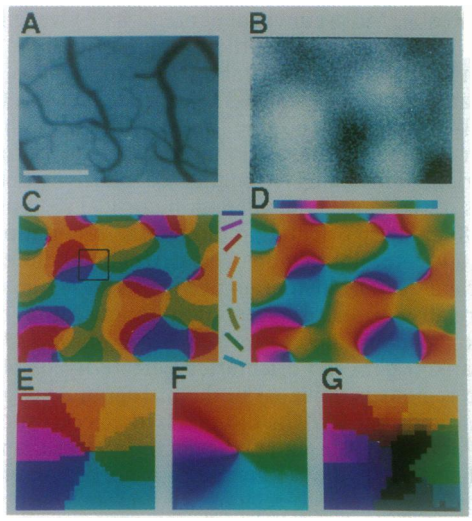

FIG. 1. Functional architecture underlying orientation preference. (*A*) Image of a ≈1.5 × 1 mm portion of macaque striate cortex. Top of the image nearly parallels the V1/V2 border. (Bar = 500 μm.) (*B*) Map of iso-orientation domains from the same portion of cortex as in *A*. Dark regions show those cortical areas that exhibit strong responses to vertical grating (90°). (*C*) Discrete angle-map of orientation preference. Oriented color bars at right indicate color code. (*D*) Continuous angle-map of orientation preference. Same unsmoothed digital data as in *C* is depicted by using the color scale shown above map. (*E*) Enlarged pinwheel (square in Fig. 1*C*). (Bar = 50 μm.) (*F*) Same pinwheel, depicted with continuous color scale of *D*. (*G*) Same pinwheel again, shown with angle-magnitude map.

indeed, changes smoothly and continuously across the cortex, except at a few points of singularity (Fig. 1*D*). This map is similar to maps obtained by Blasdel and Salama (21).

Inspection of >30 angle maps of the type shown in Fig. 1 *C* and *D*, obtained from 20 monkeys, indicated that the most prominent feature of iso-orientation domains was their radial, pinwheel-like organization (32). An enlarged image of a typical pinwheel (Fig. 1*E*) was obtained by magnifying a portion of the same angle map. It is clear that the iso-orientation domains are ordered radially around a point of singularity and that each orientation is represented just once. To show the gradual change in orientation preference, the same pinwheel (Fig. 1*E*) is also depicted using a continuous-color scale. Fig. 1*F* shows that, in a pinwheel, the orientation preference of cortical neurons changes smoothly in a radial manner around the point of singularity. Fig. 1 *D–F* (and previous results) suggest that the term iso-orientation slabs (bands) should probably be revised because discrete iso-orientation bands were not revealed even by fine electrical recordings (3, 4, 7, 21, 29).

Angle-magnitude maps show both the preferred angle, color-coded as before, and the magnitude of the response. The magnitude of the resultant vector (21, 24, 30) is represented here by the brightness of the color. Inspection of >30 angle–magnitude maps revealed that the magnitudes of the resultant vectors are small at the centers of pinwheels; this leads to a general darkening of the colors as the pinwheel center is approached, and a dark halo appears surrounding the singularity point (Fig. 1*G*). Inspection of the eight iso-orientation maps from the various stimulus orientations showed that the responses of a cell population in the vicinity of the pinwheel center were all large. To examine whether this result reflected a significant reduction of orientation tuning of single cells or was a property of a heterogeneous population, we explored the electrical response properties of single cells. Three to five unit recordings were obtained at seven singularity points, previously mapped by optical imaging *in vivo*. In >75% of such recordings, we found that the cells at or near the singularity point (within 50 μm) were sharply tuned. Thus, the darkening near the singularity point may originate from a mixture of cells with different orientation preferences in this small region.

Relationships Between Pinwheels and Ocular-Dominance Columns. We next evaluated the ocular-dominance map in the same patch of visual cortex (21, 24). The resulting map (Fig. 2*A*) shows dark and light parallel bands. These bands correspond to the right eye and left eye ocular-dominance columns, respectively. To show their relationship to the pinwheels, we first drew thin lines on the map, along the borders of ocular-dominance columns. The border regions are cortical locations at which neurons respond equally to stimulation of either eye. These borders were determined by computer analysis of the digital data and were then superimposed on the map of orientation preference (Fig. 2*B*). From this superposition, a relationship between these two functional domains became apparent: most pinwheels were nearly centered on one of the ocular-dominance columns. In maps obtained from three animals and which included 141 pinwheel centers, 81% were located along the midline of an ocular-dominance column (the midline was taken as a tenth of the column width). Most remaining pinwheel centers were located close to ocular-dominance borders, as one might expect (see *Discussion*).

A second relationship revealed here was that the iso-orientation contours tend to cross borders of ocular-dominance columns at right angles. Even in regions where ocular-dominance columns are highly curved, the principle of orthogonal crossing is maintained (see Fig. 2 *C* and *D*). Hubel and Wiesel (3) had predicted that iso-orientation bands would

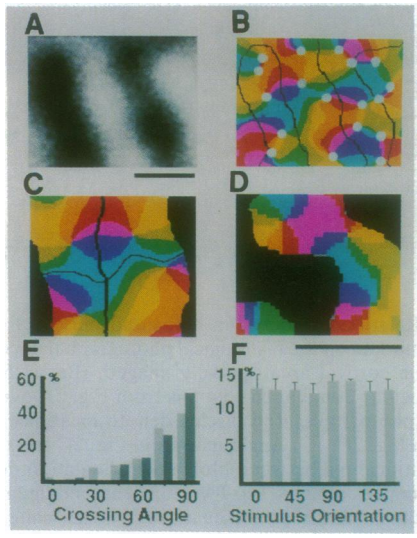

FIG. 2. Relationship between pinwheels and ocular-dominance columns. (*A*) Optical map of ocular dominance from same patch of cortex as in Fig. 1*A*. Dark bands represent columns dominated by input from the right eye, and the light bands represent columns dominated by input from the left eye. (Bar = 500 μm.) (*B*) Borders of ocular-dominance columns (from Fig. 2*A*) were overlaid onto the angle-map from Fig. 1*C*. Pinwheel centers were marked with circles (≈67% were centered on ocular-dominance columns). (*C*) Enlarged portion of *B* showing only one ocular-dominance column from each eye. The dark, thick line shows their boundary. Two pairs of connected pinwheels (clockwise and counterclockwise) are seen at top and bottom of each pair separated by the thin line. (*D*) Ocular-dominance map, taken from another monkey, in a cortical region where ocular-dominance columns were curved. Columns for the left eye were darkened to emphasize crossing angles of iso-orientation contours. (Bar = 1 mm.) (*E*) Histograms from two monkeys (light and dark bars) for crossing angles between ocular-dominance columns and iso-orientation contours. (*F*) Histogram showing percentage of cortical area devoted to each iso-orientation domain.

be orthogonal to borders of ocular-dominance columns, but this was not demonstrated in subsequent studies (6, 21). Our optical imaging has confirmed this early prediction. To quantify these observations, we have analyzed the distribution of angles at which the iso-orientation contours cross borders of ocular-dominance columns. We found that 76% of the crossing angles were between 75° and 90° (Fig. 2*E*).

Another long-standing question has been whether all iso-orientation domains are equally represented in the cortex. We found that, on average, all orientations were, in fact, equally represented (Fig. 2*F*).

Relationship Between Pinwheels and Blobs. It was also of interest to determine how the third subsystem of cells, residing in blobs (Fig. 3*A*), is related to the first two subsystems. One possibility, proposed by Gotz (33), is that the blobs are positioned exactly at the pinwheel centers. However, when locations of the blobs revealed by post-mortem cytochrome oxidase histology (Fig. 3*A*) were compared (see *Materials and Methods*) with locations of the pinwheel centers in exactly the same cortical patch, the pinwheel centers usually did not coincide with centers of blobs (Fig. 3 *B* and *C*). Upon careful inspection of three maps from two monkeys, only 17% of the 64 pinwheel centers were found inside of blobs. Most pinwheel centers (83%) were found in interblob regions or close to the borders of blobs.

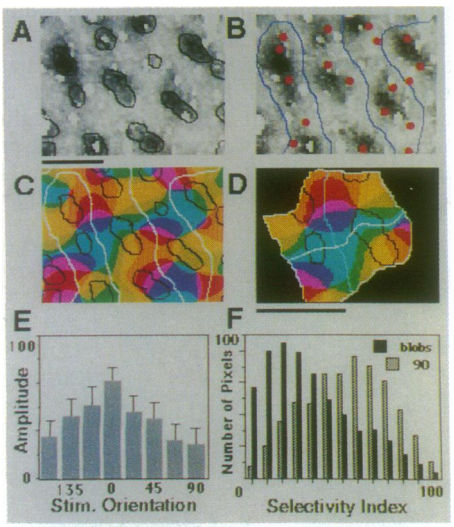

FIG. 3. Relationship between blobs and pinwheel centers. (*A*) Blobs were marked on the histological photograph that corresponded exactly to the cortical area optically imaged. (Bar = 500 μm.) (*B*) Outlines of ocular-dominance columns from Fig. 2*A* overlaid on the histological photograph. Red circles denote locations of pinwheel centers from Fig. 2*C*. (*C*) Angle-map from Fig. 2*C* and two overlays showing relationships between blobs, iso-orientation domains, and ocular-dominance columns. (*D*) Two adjacent fundamental modules, magnified from *C*. One border "separating" them (white line) divides one iso-orientation domain (light blue) into nearly equal parts, shared by the two adjacent modules. The right and left borders of the module are defined by borders of ocular-dominance columns. Each module also includes portions of blobs in it (from two to four). (Bar = 500 μm.) There are several ways to delineate borders of fundamental modules. The smooth change, in ocular dominance and in orientation preference across the upper layers of cortex (4, 7, 29), is a good example of the strategy nature has chosen; the transition between neuronal clusters exhibiting different response properties is smooth and borders are fuzzy. Therefore, our criterion for delineating borders was that the response properties of cells on either side of any border would be similar. Thus adjacent fundamental modules are continuous with one another, their fuzzy boundaries appear artificial, and these boundaries can be arbitrarily shifted along two axes, parallel to the cortical surface, by jumps of ≈0.4 mm. (*E*) Histogram of orientation tuning calculated for all cortical regions that exhibited strong responses to horizontal gratings. Stim., stimulus. (*F*) Distribution of orientation-selectivity index for blobs (dark bars) and for all cortical regions (mostly interblob regions) where large responses to vertical grating were seen (shaded bars).

The angle maps apparently show that continuous changes in orientation preference across the cortical surface (i.e., the pinwheels) were, by and large, not perturbed by the blobs. However, these angle-maps do not provide any information about orientation-tuning strength. To clarify whether the locations of the blobs coincided with cortical regions having poor (7, 8) or sharp orientation tuning, the orientation tuning in blobs and interblob regions was determined directly from the optical data. The histogram of Fig. 3*E* shows an example of the relatively sharp orientation tuning of a neuronal population in interblob regions (see *Materials and Methods*). A comparison between orientation selectivity of blobs and interblob regions is depicted in the histogram shown in Fig. 3*F*. We found that 78% of the pixels that corresponded to blobs exhibited poor orientation selectivity (less than half the maximal-selectivity index). In contrast, cortical neurons that were mostly in interblob regions were more sharply tuned. Our single-unit recordings did not encounter many neurons (<15%) with blob-like response properties, within 50 μm of the seven singularity points we investigated. It showed, once again, that the centers of pinwheels did not coincide with blobs. In addition, we noticed that our results are fully consistent with the long, tangential penetrations described by Livingstone and Hubel (7). In their data, the locations of blobs and locations of sudden and large jumps in orientation preference often did not coincide.

DISCUSSION

The Pinwheel-Like Architecture of Orientation Preference. It has been suggested on theoretical grounds that iso-orientation domains might be organized in pinwheel-like structures (32–35). The pinwheels seen here are smoothly connected to each other across the borders of ocular-dominance columns. Connected pinwheels frequently had opposite directions of orientation-preference changes—i.e., clockwise versus counterclockwise (33) (see, for example, the two pairs of pinwheels at the top of Fig. 2*C*). However, we could not find a consistent rule for the pairing of neighboring pinwheels. In some cases, we observed spurious singularity points next to ocular-dominance borders (e.g., Fig. 2*B*). Such points are formed when adjacent pinwheels, centered on two ocular-dominance columns, are connected in a certain way (e.g., a 2 × 2 arrangement of four clockwise pinwheels creates a spurious counterclockwise pinwheel on the boundary of the two ocular-dominance columns). During development some points centered on some patches of ocular-dominance columns apparently behave like a seed for a crystal around which the orderly petals of various iso-orientation domains form pinwheels. Such a developmental process, probably a dynamic one, requires only short-range interactions of up to 400 μm. In contrast, maintaining an orderly arrangement for clockwise and counterclockwise pinwheels, such as depicted in Gotz models (33), requires a much greater interaction range and a formidable remodeling of synaptic connections during development. In general, the pinwheel organization of orientation preference in monkey primary visual cortex is very similar to that seen in cat areas 17 and 18 by Bonhoeffer and Grinvald (29), who confirmed and extended earlier electrophysiological mapping of pinwheels by Swindale *et al.* (36).

Is Monkey Primary Visual Cortex Composed of a Regular Mosaic of Repeating Fundamental Modules? Here we define a fundamental module as the smallest cortical area that includes a complete representation of each of the three subsystems. This term is probably related to hypercolumns (4), a term that has been used by many authors to describe various types of repeating modules and, therefore, became somewhat ambiguous.

An intriguing question has been whether the cortex is built of repeating fundamental modules. A nearly perfect mosaic of repeating modules was observed here only for a submodule, composed of a pinwheel centered on a patch of an ocular-dominance column. Such "monocular" pinwheels are continuous with one another, along and across ocular-dominance boundaries. Given that a pinwheel can process visual information derived from all orientations, detected by one eye, one might suspect that two adjacent patches of complementing ocularity, each containing one pinwheel and portions of a few blobs, form the fundamental processing module in primary visual cortex. Many such fundamental modules were, indeed, found; an enlarged portion of a map (Fig. 3*B*), focusing on two adjacent fundamental modules, is depicted in Fig. 3*C*. However, at present we could not define a fundamental module in a way that would result in a regular mosaic of repeating units as defined above.

Several of the findings and interpretations described here differ in important respects from those of Blasdel and Salama (21). Although pinwheels can be seen in their data, they did not comment on their prominence. Furthermore, their more recent model of cortical organization shows singularities as well as a full set of parallel slabs (30). Their model is not consistent with the existence of a single pinwheel, because the stacks of parallel iso-orientation slabs cover the complete orientation-preference range along one axis rather than radially (30). In addition, Blasdel and Salama (21) rejected the notion that iso-orientation contours cross borders of ocular-dominance columns at approximately right angles. In the context of fundamental modules, they proposed that loop-like fractures delineate the borders of processing modules, even though some orientations were not always represented within those modules.

Multiple Mosaics of All Subsystems as an Alternative to a Single Mosaic of Fundamental Modules. It appears either that we failed to see the regular mosaic-like arrangement of fundamental modules hidden in our data or that such an arrangement does not exist in the primary visual cortex of the macaque monkey. What we see in our data is a mosaic-like arrangement of blobs and mosaic-like arrangements for each of the partially overlapping iso-orientation domains. The mosaics of each iso-orientation patches are actually reminiscent of the mosaic of blobs. For examples of these mosaic-like patches of iso-orientation domains, demonstrated over a larger cortical area than shown here (Fig. 1*B*), compare figure 29-12B of ref. 37, showing four different mosaics of iso-orientation domains, with figure 29-13, showing the mosaic-like patches of blobs.

Hubel and Wiesel (4) showed that, during tangential penetrations, the electrode must be advanced ≈2 mm across the cortical surface (≈two hypercolumns) to locate cells that do not have overlapping receptive fields. The size of each "fundamental module" we detected was ≈800 μm × 400 μm (eccentricity of 6–8° close to the V1/V2 border). Thus at least four fundamental modules (2 × 2) are processing some information from a single point of a retinal image, in parallel (in the upper cortical layers). In such a large area, we observed a redundancy of the individual domains contained in the regular mosaics of blobs and of iso-orientation domains. This organization of subsystems can serve at least two important objectives. (*i*) The redundancy can functionally compensate for imperfections in the mosaic-like layout of fundamental modules. A regular mosaic of fundamental modules is actually not required because regular mosaics of all the individual subsystems are adequately represented. (*ii*) This redundancy provides an abundant neuronal substrate for local computations and population coding of the complex visual scene thoroughly analyzed by the primate visual cortex.

Note Added in Proof. Two recent publications have addressed some of these topics (38, 39).

We thank Drs. D. Y. Ts'o, D. Malonek, C. D. Gilbert, and T. N. Wiesel for their contributions, and Drs. R. Tootell, E. Kaplan, L. C. Katz, and D. Purves for their useful comments. This work was supported by Margaret Enoch and the Schilling Foundation.

1. Mountcastle, B. (1957) *J. Neurophysiol.* **20,** 408–434.
2. Hubel, D. H. & Wiesel, T. N. (1968) *J. Physiol. (London)* **195,** 215–243.
3. Hubel, D. H. & Wiesel, T. N. (1974) *J. Comp. Neurol.* **158,** 267–294.
4. Hubel, D. H. & Wiesel, T. N. (1977) *Proc. R. Soc. London B* **198,** 1–59.
5. Levay, S., Hubel, D. H. & Wiesel, T. N. (1975) *J. Comp. Neurol.* **159,** 559–576.
6. Hubel, D. H., Wiesel, T. N. & Stryker, M. P. (1978) *J. Comp. Neurol.* **177,** 361–380.
7. Livingstone, M. S. & Hubel, D. H. (1984) *J. Neurosci.* **4,** 309–380.
8. Ts'o, D. Y. & Gilbert, C. D. (1988) *J. Neurosci.* **8,** 1712–1727.
9. Tootell, R. B. H., Silverman, M. S., Hamilton, S. L., Switkes, E. & De Valois, R. L. (1988) *J. Neurosci.* **8,** 1610–1624.
10. Horton, C. H. & Hubel, D. H. (1981) *Nature (London)* **292,** 762–764.
11. Grinvald, A., Manker, A. & Segal, M. (1982) *J. Physiol. (London)* **333,** 269–291.
12. Orbach, H. S. & Cohen, L. B. (1983) *J. Neurosci.* **3,** 2251–2262.
13. Grinvald, A., Anglister, L., Freeman, J. A., Hildesheim, R. & Manker, A. (1984) *Nature (London)* **308,** 848–850.
14. Orbach, H. S., Cohen, L. B. & Grinvald, A. (1985) *J. Neurosci.* **5,** 1886–1895.
15. Tasaki, I., Watanabe, A., Sandlin, R. & Carnay, L. (1968) *Proc. Natl. Acad. Sci. USA* **61,** 883–888.
16. Salzberg, B. M., Davila, H. V. & Cohen, L. B. (1973) *Nature (London)* **246,** 508–509.
17. Cohen, L. B., Salzberg, B. M., Davila, H. V., Ross, W. N., Landowne, D., Waggoner, A. S. & Wang, C. H. (1974) *J. Membr. Biol.* **19,** 1–36.
18. Grinvald, A., Salzberg, B. M. & Cohen, L. B. (1977) *Nature (London)* **268,** 140–142.
19. Waggoner, A. S. & Grinvald, A. (1977) *Ann. N.Y. Acad. Sci.* **303,** 217–242.
20. Grinvald, A., Frostig, R. Lieke, E. E. & Hildesheim, R. (1988) *Phys. Rev.* **68,** 1285–1366.
21. Blasdel, G. G. & Salama, G. (1986) *Nature (London)* **321,** 579–585.
22. Grinvald, A., Lieke, E., Frostig, R. D., Gilbert, C. D. & Wiesel, T. N. (1986) *Nature (London)* **324,** 361–364.
23. Frostig, R. D., Lieke, E. E., Ts'o, D. Y. & Grinvald, A. (1990) *Proc. Natl. Acad. Sci. USA* **87,** 6082–6086.
24. Ts'o, D. Y., Frostig, R. D., Lieke, E. E. & Grinvald, A. (1990) *Science* **249,** 417–420.
25. Hill, D. K. & Keynes, R. D. (1949) *J. Physiol. (London)* **108,** 278–281.
26. Chance, B., Cohen, P., Jobsis, F. & Schoener, B. (1962) *Science* **137,** 499–508.
27. Jobsis, F. F., Keizer, J. H., LaManna, J. C. & Rosental, M. J. (1977) *J. Appl. Physiol.* **43,** 858–872.
28. Grinvald, A., Frostig, R. D., Siegal, R. M. & Bartfeld, E. (1991) *Proc. Natl. Acad. Sci. USA* **88,** 11559–11563.
29. Bonhoeffer, T. & Grinvald, A. (1991) *Nature (London)* **353,** 429–431.
30. Blasdel, G. G. (1989) in *Sensory Processing in the Mammalian Brain: Neural Substrates and Experimental Strategies*, ed., Lund, J. S. (Oxford Univ. Press, Oxford UP), pp. 242–268.
31. Ratzlaff, E. H. & Grinvald, A. (1991) *J. Neurosci. Methods* **36,** 127–137.
32. Braitenberg, V. & Braitenberg, C. (1979) *Biol. Cybern.* **33,** 179–186.
33. Gotz, K. G. (1988) *Biol. Cybern.* **58,** 213–223.
34. Swindale, N. V. (1982) *Proc. R. Soc. London B* **215,** 211–230.
35. Linsker, R. (1986) *Proc. Natl. Acad. Sci. USA* **83,** 8779–8783.
36. Swindale, N. V., Matsubara, J. A. & Synader, M. S. (1987) *J. Neurosci.* **7,** 1414–1427.
37. Kandel, E. R. (1991) in *Principles of Neural Science*, eds. Kandel, E. R., Schwartz, J. H. & Jessel, T. J. (Elsevier, London), 3rd Ed., p. 432.
38. Blasdel, G. G. (1992) *J. Neurosci.* **12,** 3115–3138.
39. Blasdel, G. G. (1992) *J. Neurosci.* **12,** 3139–3161.